Biomass Conversion and Biorefinery (2024) 14:19929–19946
https://doi.org/10.1007/s13399-023-04161-5

ORIGINAL ARTICLE

Chemically modified *Azadirachta indica* sawdust for adsorption of methylene blue from aqueous solutions

Zeeshan Ahamad[1] · Mohsina Ahmed[1] · Fouzia Mashkoor[2] · Abu Nasar[1]

Received: 11 January 2023 / Revised: 16 March 2023 / Accepted: 29 March 2023 / Published online: 12 April 2023

Abstract

This study explores the competency of *Azadirachta indica* sawdust (A.I.S.D.) and NaOH-modified *Azadirachta indica* sawdust (N.A.I.S.D.) as the prospective adsorbents for the removal of methylene blue (M.B.) from aqueous solution. Prepared adsorbents were characterized by performing S.E.M./E.D.X.S., T.E.M./S.A.E.D., B.E.T., F.T.I.R., T.G.A.–D.T.G., X.R.D., pH_{pzc} (point of zero charge), proximate, and component analyses. The proximate analysis indicates that N.A.I.S.D. has higher fixed carbon and cellulose, and lower ash, volatile matter, moisture, hemicellulose, extractive, and lignin than A.I.S.D. The operational parameters (contact time, pH, temperature, amount of adsorbent, and initial dye concentration) were varied. It was found that the equilibrium for the optimum dye removal was achieved in 120 and 75 min for A.I.S.D. and N.A.I.S.D., respectively. Numerous isotherm and kinetic frameworks were used to assess the experimental results. The adsorption of M.B. followed a Langmuir adsorption isotherm and pseudo-second-order kinetics. The thermodynamic variables, such as changes in free energy (ΔG°), entropy (ΔS°), and enthalpy (ΔH°) of adsorption, were assessed. Adsorption by both adsorbents was feasible, endothermic, and associated with an increase in entropy. Four adsorption–desorption cycles of M.B.-loaded A.I.S.D. and N.A.I.S.D. were successfully performed using HCl as a desorbing agent. The finding shows that N.A.I.S.D. is a cost-effective and efficient adsorbent for eliminating M.B. from an aqueous medium.

Keywords *Azadirachta indica* sawdust · Methylene blue · Adsorptive removal · NaOH modification

1 Introduction

Water pollution has been a significant problem for many years [1]. However, it was inevitable due to the industrial revolution, globalization, and the application of science, which caused irreversible environmental damage [2]. As a result of the increased misuse of water in a plethora of agricultural, household, and industrial sectors, drinking water quality and availability are deteriorating and causing concern globally [3]. Industrial runoff contains herbicides, insecticides, fungicides, heavy metals, dyes, drugs, and other organic and inorganic pollutants that are innately eco-pernicious and imperishable [4–7]. Among all these pollutants, dyes are a colorful contaminant widely employed in various industries like paint, automobile, paper, chemical, polymer, cosmetic, textile, pharmaceutical, leather, and printing [8–11]. The textile industry consumes considerable water during manufacturing, releasing large amounts of dye-loaded effluents into freshwater sources [12]. It is well-known that these dyes also show a lasting adverse impact on marine species.

Highlights
- Chemical modification of *Azadirachta indica* sawdust produced a novel adsorbent.
- Langmuir adsorption isotherm and pseudo second order kinetics models were obeyed.
- M.B. adsorption was feasible, endothermic, and accompanying with entropy increase.
- The adsorbents could be regenerated and reused for up to four repeated cycles.
- Large numbers of micropores have been developed on the surface after the treatment.

✉ Abu Nasar
abunasaramu@gmail.com

[1] Department of Applied Chemistry, Faculty of Engineering and Technology, Aligarh Muslim University, Aligarh 202002, India

[2] School of Mechanical Engineering, Yeungnam University, Gyeongsan, Gyeongbuk 38541, Republic of Korea

Furthermore, dyes also disrupt photosynthetic processes by preventing sunlight from reaching aquatic ecosystems, which, in turn, significantly impacts the aquatic ecosystem [13, 14]. Among several toxic dyes, methylene blue (M.B.) is a typical cationic dye that gives a blue hue when dissolved in water. It is widely used in dye industries for coloring cotton, silk, wool, etc., and in pharmaceutical and chemical industries. Although M.B. has many practical uses, long-time exposure to it can irritate the skin with redness, fever, high blood pressure, itching, mouth irritation, dizziness, throat, stomach, gastrointestinal and esophagus pain, diarrhea, headache, nausea, and vomiting. Therefore, M.B. containing effluent should be treated adequately before discharge into water bodies.

The decontamination of dyes from aqueous medium has been frequently accomplished using various methods like membrane filtration, ion exchange, photocatalytic process, biological treatment (aerobic and anaerobic), electrodialysis, coagulation and flocculation, Fenton oxidation, reverse osmosis, ozonation, adsorption, etc. Each method has specific merits and demerits and has been discussed in several review papers [15–20]. Most methods have shown their applicability in treating dye-contaminated water at laboratory scales. Still, they suffer from the drawbacks of their large-scale relevance due to high cost, the requirement of high energy consumption, large operational time, and the possible generation of large quantities of secondary sludge [21]. Thus, the selection of an appropriate method has always been a challenging task. Among the several ways, the adsorption technique has received considerable attention as it is greener, cleaner, cheaper, simpler, and flexible in operation, non-sensitive to toxic pollutants [22, 23].

Furthermore, this technique has minimum sludge generation and disposal problems and has provision for adsorbent recovery. However, choosing an appropriate adsorbent depends upon the presence of reactive functional groups on its surface and surface area. The silica gel and activated carbon have been acknowledged as conventional adsorbents, which show outstanding adsorption capacity towards various pollutants. But, their applications are not always feasible because of the significant expense and issue of adsorbent regeneration. Accordingly, research has focused on searching for more cost-effective and efficient adsorbents. Biomass wastes, which include agricultural residues, natural materials, and food/domestic wastes, are renewable resources that might be used to make high-value carbon products proving to be viable alternatives for adsorption applications. Over the past few years, several types of adsorbents made from vegetal and animal residues like stems, peels, sawdust, nut shells, barks, egg shells, bird plumes, leaves, husks, and additional analogous residues have been used as value-added products to eliminate or reduce the hazardous pollutants from wastewater [23–32]. Biomass wastes have negligible or no commercial value and frequently have disposal issues. Thus, employing these wastes as adsorbents may add their economic value and decrease disposal costs. But, biomass-based adsorbent materials have restricted applications due to their specificity and poor adsorption capacity. The limitations of biomass-based adsorbents can be overcome by chemically modifying them. Various reagents, like alkalis, acids, surfactants, polymers, etc., were used as modifying agents to enhance adsorption efficiency. Furthermore, the choice of modifying agents is based on several factors, including the type of the substance, contamination, affordability, and adsorption efficacy under the given experimental parameters.

Herein, sawdust (SD) of the *Azadirachta indica* (Neem) tree has been chemically modified by NaOH to synthesize a novel adsorbent to eliminate hazardous dye from an aqueous solution. Since sawdust is a waste found in abundance, it could be used as a prospective and inexpensive adsorbent for the low-cost treatment of dye-laden water. This study explores the possible exploitation of untreated *Azadirachta indica* sawdust (A.I.S.D.) and NaOH-modified *Azadirachta indica* sawdust (N.A.I.S.D.) adsorbents that may be effectively used for dye sequestration from artificially contaminated water.

Given the above facts, the present research has been planned with a prima facie to utilize A.I.S.D. and N.A.I.S.D. adsorbents to purify wastewater effectively. A technique for evaluating complete operational parameters was developed, and A.I.S.D. and NaOH-treated A.I.S.D. (N.A.I.S.D.) were employed for the sequestration of M.B. dye. A maximum outcome has been achieved by optimizing laboratory parameters, viz., solution pH, amount of adsorbent, contact time, temperature, and initial dye concentrations. Furthermore, S.E.M./E.D.X.S., T.E.M./S.A.E.D., B.E.T., T.G.A.–D.T.G., X.R.D., pH_{pzc}, and F.T.I.R. characterizations of A.I.S.D. and N.A.I.S.D., and thermodynamic, isothermal, and kinetic analyses of experimental data were also carried out.

2 Experimental procedure

2.1 Materials

Analytical reagent grade reagents and chemicals (HCl, KNO_3, CH_3OH, H_2SO_4, NaOH, C_6H_6, CH_3COOH), and microscopic grade M.B., obtained from CDH, India, were used in this study. In all the experimental studies, demineralized water purified by double distillation (DM-DW) was used. A stock solution of dye (1000 mg L^{-1}) was prepared by dissolving a befitting quantity in the DM-DW.

2.2 Adsorbents preparation

Azadirachta indica sawdust waste, procured from a nearby sawmill, was washed vigorously with DM-DW to remove superficially tenacious dust and solvable contaminations. After that, it was dried in a 90 °C oven for 12 h until completely dry. Afterward, the dried mass was powdered using a mixer grinder and passed through a sieve with 80 BSS mesh size. The resulting material was then repeatedly washed with DM-DW. After filtering, the powder was dried in an oven for 12 h at 90 °C. The chemical treatment of the A.I.S.D. was executed by using 0.1 M sodium hydroxide with a 1:5 proportion (A.I.S.D.: alkali, w/v) with 8 h of continuous mixing at ambient temperature. Afterward, the mass was screened using Whatman filter paper by suction filtration and washed many times with DM-DW to discard unreacted sodium hydroxide. Then, N.A.I.S.D. was kept for 8 h at 90 °C in an oven. The adsorbents (A.I.S.D. and N.A.I.S.D.) so prepared were pulverized with a mortar and pestle into powder form and stored in airtight vials under desiccated conditions for future usage.

2.3 Adsorbents characterization

2.3.1 Proximate analysis

A.I.S.D. and N.A.I.S.D. were subjected to proximate analysis to obtain quantitative values about moisture, volatile matter, ash, and fixed carbon employing the reported techniques [33–35].

Moisture The moisture percentage in A.I.S.D. and N.A.I.S.D. was calculated by taking 1.0 g of each adsorbent and kept in a crucible made of porcelain at 100 °C for 60 min. After that, the crucible was removed from the oven and kept in a dry environment for cooling. The sample weight (wt) loss was measured by weighing the sample, and the % moisture content (%M) was calculated by using the following equation:

$$\% \, \mathrm{M} = \frac{\text{sample wt loss}}{\text{sample initial wt}} \times 100 \tag{1}$$

Ash The percentage of ash in A.I.S.D. and N.A.I.S.D. was determined by taking 1.0 g of each adsorbent, placing it in a ceramic crucible, and kept inside a muffle furnace at 680 °C for 6 h. Afterward, the ash was carefully taken out with the help of heat-resistant furnace gloves and kept in a dry environment for cooling. The weight of the sample was recorded, and the percentage of ash (%A) was calculated by employing the following expression:

$$\% \, \mathrm{A} = \frac{\text{ash wt}}{\text{adsorbent wt}} \times 100 \tag{2}$$

Volatile matter The percentage of volatile content in A.I.S.D. and N.A.I.S.D. was measured by taking 1.0 g of each adsorbent. A muffle furnace was used to heat it for 12 min at about 610 °C in a crucible. After carefully taking it out and waiting till the sample returned to its normal temperature, the weight of the adsorbent was recorded, and the percentage of volatile content (%V) was calculated using the following expression:

$$\% \, \mathrm{V} = \frac{\text{Initial wt} - \text{final wt}}{\text{Initial wt}} \times 100 \tag{3}$$

Fixed carbon For the quantitative calculation of percentage fixed carbon (%V), the following expression was used:

$$\%\mathrm{FC} = 100 - \%(\mathrm{A} + \mathrm{M} + \mathrm{V}) \tag{4}$$

2.3.2 Analysis of components

The analysis of components in A.I.S.D. and N.A.I.S.D. was performed by already reported techniques [33, 36]:

Extractives In the extractive analysis of A.I.S.D. and N.A.I.S.D., each sample having the initial weight of M_i was treated separately using ethanol and benzene combination (1:2) at 30 °C for 4 h. After that, the samples were filtered, and the residue was dried at 90 °C until fully dry. The weight of the residue (M_r) was measured after keeping it in a dry environment for 5 h. The percentage of extractives (%E) was estimated using the expression:

$$\%\mathrm{E} = \frac{\mathrm{M_i} - \mathrm{M_r}}{\mathrm{M_i}} \times 100 \tag{5}$$

Hemicellulose The residue of extractive analysis (M_a) was refluxed for 6 h with a 250 mL solution of 0.5 M sodium hydroxide. After filtering, the weight of the residue (M_b, g) was used to determine the hemicellulose (% H) by using the expression:

$$\%\mathrm{H} = \frac{\mathrm{M_a} - \mathrm{M_b}}{\mathrm{M_a}} \times 100 \tag{6}$$

Lignin M_c g of the residue of extractive analysis was treated with 25 ml H_2SO_4 for 20 h at 14 °C, and then the mixture was diluted with DM-DW to 250 mL and refluxed for 1 h. After filtering, the residual mass was washed with DM-DW several times to remove the SO_4^{2-}. Finally, the weight of this oven-dried residue (M_d) obtained in this way was used to evaluate the amount of lignin which was evaluated from the oven-dried mass of the residue using the following equation:

$$\%L = \frac{M_d(1-E)}{M_c} \times 100 \quad (7)$$

Cellulose The percentages of cellulose were estimated using the expression:

$$\%C = 100 - (A + E + L + H)\% \quad (8)$$

2.3.3 Point of zero charge

The point of zero charge (pH_{pzc}) of N.A.I.S.D. was determined using the solid addition technique. This was carried out by taking 25 mL of 0.1 M KNO_3 in various 100 mL beakers. By the drop-by-drop addition of 0.1 M HCl/NaOH in solutions, the initial pH (pH_i) was adjusted from 2 to 13. Following that, 0.05 g of adsorbent was added to each beaker, which was then properly enclosed and left in the dark for 48 h. The plot of ΔpH (pH_f-pH_i) vs. pH_i was used to evaluate pH_{pzc} of N.A.I.S.D.

2.3.4 Instrumental analyses

S.E.M. (scanning electron microscopy) and E.D.X.S. (energy dispersive X-ray) analyses (JEOL, JSM-6510LV, Japan) were utilized to investigate morphologic characteristics of the adsorbents. The T.E.M. was used to investigate adsorbent particle shape and size (JEOL, 2100). The pore volume and surface area were determined by employing B.E.T. analyzer (Autosorb IQ2, Quantachrome Instruments, USA). X.R.D. was used to investigate the crystallinity or amorphous nature of the adsorbents (SmartLab, Rigaku, Japan). The experiments were conducted in the 5–80° (2θ) range at a 20°/min scan rate with a 0.02° step size. Fourier transform infrared (F.T.I.R.) spectrometer (1800 IR spectrophotometer, Perkin-Elmer) was used to analyze the functional groups of the adsorbent in the spectrum region of 4000–400 cm^{-1}. In a nitrogen environment, T.G.A.–D.T.G. was performed in a thermogravimetric analyzer (Perkin Elmer thermal analysis instruments) in a temperature range of 24 to 750 °C with a controlled heating rate of 20 °C min^{-1}. The weight loss of the adsorbents as a function of temperature was measured in this study owing to the degradation of their components.

2.3.5 Batch adsorption studies

Batch adsorption was utilized to optimize the efficacy of the adsorbent in removing M.B. from synthetically contaminated water. Batch experiments were conducted in 100 mL beakers containing 25 mL dye solution with 0.01 g of adsorbent (A.I.S.D. or N.A.I.S.D.) at the solution pH 7. After attaining equilibrium or adsorption at any desired time t, the residual concentration of M.B. was measured by a UV–vis spectrophotometer at a λ_{max} of 665 nm. The equilibrium adsorption capacity (q_e) and removal efficiency (%R) were obtained by using the following equations:

$$q_e = (C_o - C_e) \times \frac{V}{M} \quad (9)$$

$$\%R = \frac{(C_0 - C_t)}{C_0} \times 100 \quad (10)$$

In the above equations, C_o, C_e, and C_t are the starting, equilibrium, and any-time concentrations (mg L^{-1}) of M.B. in solution, V is the volume (L) of M.B. solution, and M (g) is the weight of A.I.S.D. or N.A.I.S.D., respectively. A similar equation obtained by replacing the term C_e with C_t in Eq. (9) was used to compute the adsorption capacity (q_t) at any time t.

2.3.6 Regeneration and desorption experiments

It is essential to regenerate the used adsorbent several times before its disposal to make the overall treatment process as cost-effective as possible. A variety of desorbing agents, such as HCl, NaOH, CH_3COOH, NaCl, and water (DM-DW), were used to explore this possibility. M.B.-loaded A.I.S.D. and N.A.I.S.D. were extensively cleaned with DM-DW to remove the unadsorbed dye. The M.B.-loaded A.I.S.D. and N.A.I.S.D. were then agitated separately with 25 mL of each desorbing agent for 4 h and then filtered. Thereafter, the supernatant was analyzed, and percent desorption (%D) was computed by using the following relation:

$$\%\text{Desorption} = \frac{m_d}{m_a} \times 100 \quad (11)$$

Here, m_d and m_a in mg L^{-1} are the desorbed and adsorbed M.B. concentrations, respectively.

3 Results and discussion

3.1 Proximate and component analysis of A.I.S.D. and N.A.I.S.D.

The outcomes of proximate and constituent analyses of the N.A.I.S.D. and A.I.S.D. shown in Table 1 clearly show the compositional alteration of A.I.S.D by NaOH modification. N.A.I.S.D. has enhanced fixed carbon and cellulose content while decreasing hemicelluloses, moisture, lignin, volatile matter, extractive, and ash content. In the presence of heat, the decomposition of hemicellulose and cellulose occurs in 150 to 350 °C and 250 to 400 °C temperature ranges, respectively, whereas lignin decomposes gradually in the range of 250 to 600 °C [37]. Thus, in light of compositional change, one may conclude that N.A.I.S.D. has more temperature tolerance than A.I.S.D.

3.2 S.E.M./E.D.X.S. analyses

Figure 1a and c show the S.E.M. micrographs (×5000) of A.I.S.D. and N.A.I.S.D. Upon M.B. adsorption, the variations on the exterior of these adsorbent materials are seen respectively in Fig. 1b and d. The porosity and uneven surface of A.I.S.D. are noticeable in S.E.M. micrographs. The adsorbent, N.A.I.S.D., exhibited more empty sites due to the NaOH modification as alteration provided the formation of a large number of micropores. During the modification process, some contaminants were also possibly eliminated. Dye molecules were trapped and adsorbed more easily on the surface of N.A.I.S.D. due to newly created pores. Figure 1b and d suggest that the molecules were filled in pores and micropores of N.A.I.S.D. surface. The E.D.X.S. spectra of loaded M.B. onto A.I.S.D. and N.A.I.S.D. are shown respectively in Fig. 1e and f which indicate the presence of Cl. In addition to C, N, and O, the presence of Cl suggest the successful adsorption of M.B. ($C_{16}H_{18}N_3SCl$).

3.3 T.E.M. analysis

T.E.M. analysis was used to investigate the structural aspects of N.A.I.S.D. The T.E.M. image shown in Fig. 2a shows that the particles of N.A.I.S.D. are in the nano range (6–16 nm), which are much smaller than that found for A.I.S.D. (16–42) nm [38]. The presence of nanometer-ranged particles indicated a higher exposed surface area for effective sequestration of M.B. dye. In earlier work, a diffused pattern in the selected area electron diffraction (S.A.E.D.) of A.I.S.D. was observed, which pointed out the amorphous nature of A.I.S.D. [38]. While in the case of N.A.I.S.D., the appearance of bright diffraction rings in the S.A.E.D. pattern (Fig. 2b) indicates that N.A.I.S.D. has a somewhat greater degree of crystallinity than A.I.S.D. It was due to an increase in cellulose content.

3.4 B.E.T. analysis

A good surface area of 3.149 $m^2\ g^{-1}$ was obtained for N.A.I.S.D. This value is higher than the value of 2.507 m^2g^{-1} as observed for the unmodified adsorbent based on the same raw material, i.e., A.I.S.D. [38]. The summary of surface area and pore analysis of N.A.I.S.D. are summarized in Table 2. The B.E.T. nitrogen adsorption–desorption isotherms at 77 K, along with the BJH pore size distribution adsorption plot, are depicted in Fig. 2c. The improved surface characteristics of N.A.I.S.D. over A.I.S.D. have also been reflected in the proximate and constituent analyses of both adsorbents as the former contains a higher content of cellulose and fixed carbon, and lower in the volatile matter, hemicellulose, and lignin (Table 1).

Table 1 Proximate and constituent analyses of A.I.S.D. and N.A.I.S.D.

Components	A.I.S.D.	N.A.I.S.D.
Volatile matter (%)	55.23	45.21
Fixed carbon (%)	26.98	30.25
Extractive (%)	10.62	6.80
Moisture(%)	7.60	5.50
Cellulose (%)	45.65	57.23
Hemicellulose (%)	24.58	20.54
Ash (%)	1.60	0.28
Lignin (%)	17.54	15.15

3.5 X.R.D. analysis

Figure 2d shows X.R.D. result from 5 to 80° range of 2θ, indicating that the current adsorbent is a low crystalline material. The amorphous nature of the adsorbent is due to the presence of hemicelluloses and lignin [33]. The three peaks seen in the 2θ range at 6.48°, 22.08°, and 34.12° are because of the presence of cellulose in the biomass. The prominent peaks at around 16° and 22° were also reported on different sawdust-based adsorbents, viz., rubber wood [39], pinewood [40, 41], *Tectona grandis* [42], *Pinus elliotii* [43], *Cunninghamia lanceolata* [44], massaranduba [45], etc.

3.6 T.G.A.–D.T.G. analysis

The T.G.A. thermogram of N.A.I.S.D. shown in Fig. 2(d-inset) is represented by many stages, namely the evolution of moisture and the decomposition of hemicellulose, cellulose, and lignin. The moisture evolution occurs in the lowest temperature range, followed by decomposing the most unstable biomass component, hemicellulose. The cellulose decomposes at a higher temperature, while lignin decomposition starts even from very low temperatures and continues up to 900 °C. However, there is no general agreement in the temperature ranges for the decomposition of components of different biomasses. For example, for different biomasses, the temperature ranges for the moisture evolution and decomposition of hemicellulose, cellulose, and lignin were reported in vast ranges, typically 50–200, 50–400, 240–588, and 160–900 °C, respectively [45–51]. The D.T.G. thermogram (Fig. 2d-inset) clearly shows the maxima occurring at 353.18 °C.

3.7 F.T.I.R. analysis

F.T.I.R. spectra were used to understand better the availability of distinct functional groups on the adsorbent

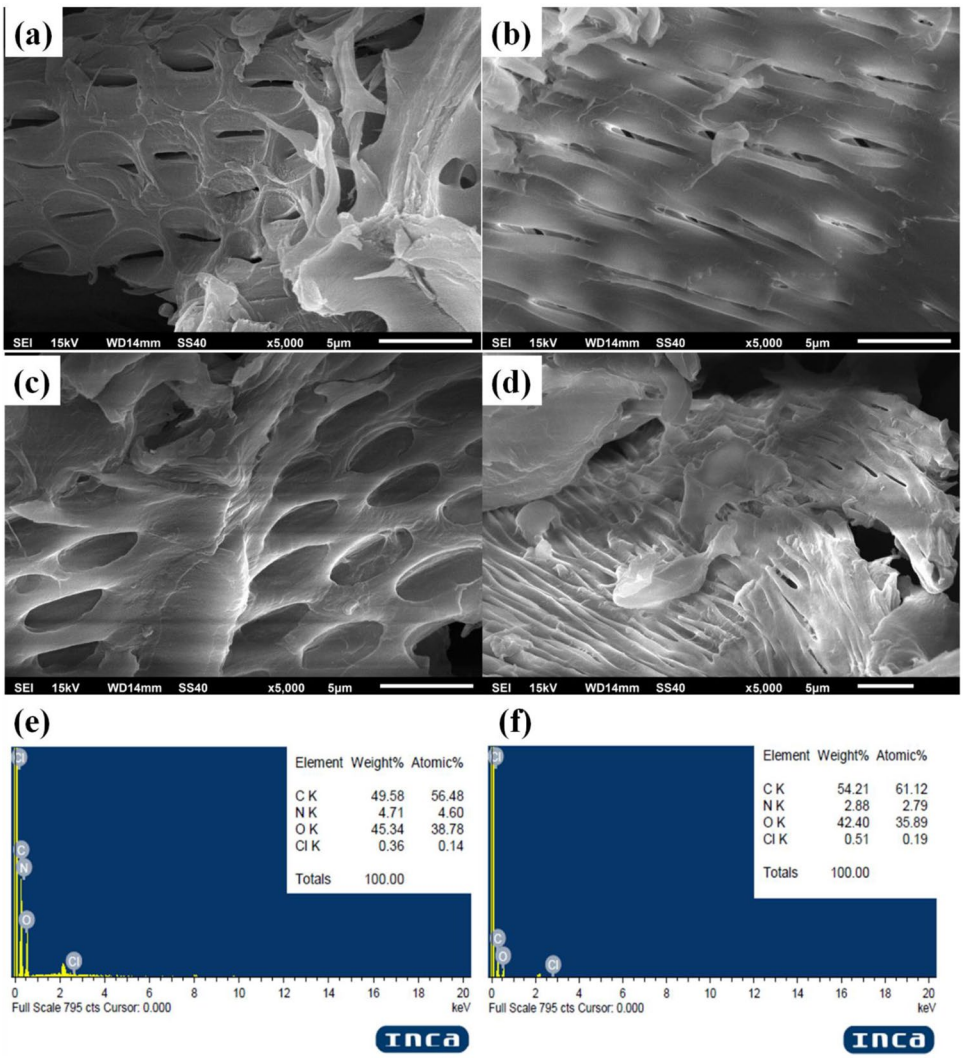

Fig. 1 S.E.M. micrographs of **a** A.I.S.D., **b** A.I.S.D./M.B., **c** N.A.I.S.D., and **d** N.A.I.S.D./M.B; E.D.X.S. results of **e** A.I.S.D./M.B. and **f** N.A.I.S.D./M.B

surface. The strong peak at 3443 cm^{-1} (Fig. 3a) observed in N.A.I.S.D. represents the –OH stretching of the phenolic group of cellulose and lignin, and the peak at 2960 cm^{-1} indicates the presence of $–CH_2$ stretching of the aliphatic compound [52]. The peak at 2147 cm^{-1} indicates the presence of N–H stretching. The arrival of peaks at 1735 cm^{-1} and 1642 cm^{-1} specifies the presence of C = O stretching of the aldehyde group and C = C stretching of the phenolic group, respectively [41]. Peaks at 1477 cm^{-1}, 1402 cm^{-1}, 1282 cm^{-1}, and 1131 cm^{-1} in the N.A.I.S.D. spectra can be due to $-CH_2$ bending, – OH bending, and – C – O stretching of the phenolic group and six-member cyclic ether group, respectively [41]. The changes in position and intensity of these peaks after the adsorption of M.B. signify the involvement of the stated groups in the binding of M.B. with N.A.I.S.D. during the adsorption process.

3.8 Study of operational parameters

3.8.1 Initial dye concentration (C_o) and contact time

The effect of contact time on the adsorption capacity of A.I.S.D. and N.A.I.S.D. towards M.B. at different initial concentrations (100, 150, and 200 mg L^{-1}) of M.B. is shown in Fig. 3b at a typical temperature of 303 K. The plot demonstrates that the initial 20 min shows a significant rise in the adsorption capacity followed by a slower increase of the dye removal until it achieves equilibrium in around 120 min and 75 min for A.I.S.D. and N.A.I.S.D., respectively. The rapid increase in adsorption capacity during the initial stage by both adsorbents is because of the abundance of a significant proportion of unoccupied sites on the adsorbent surface.

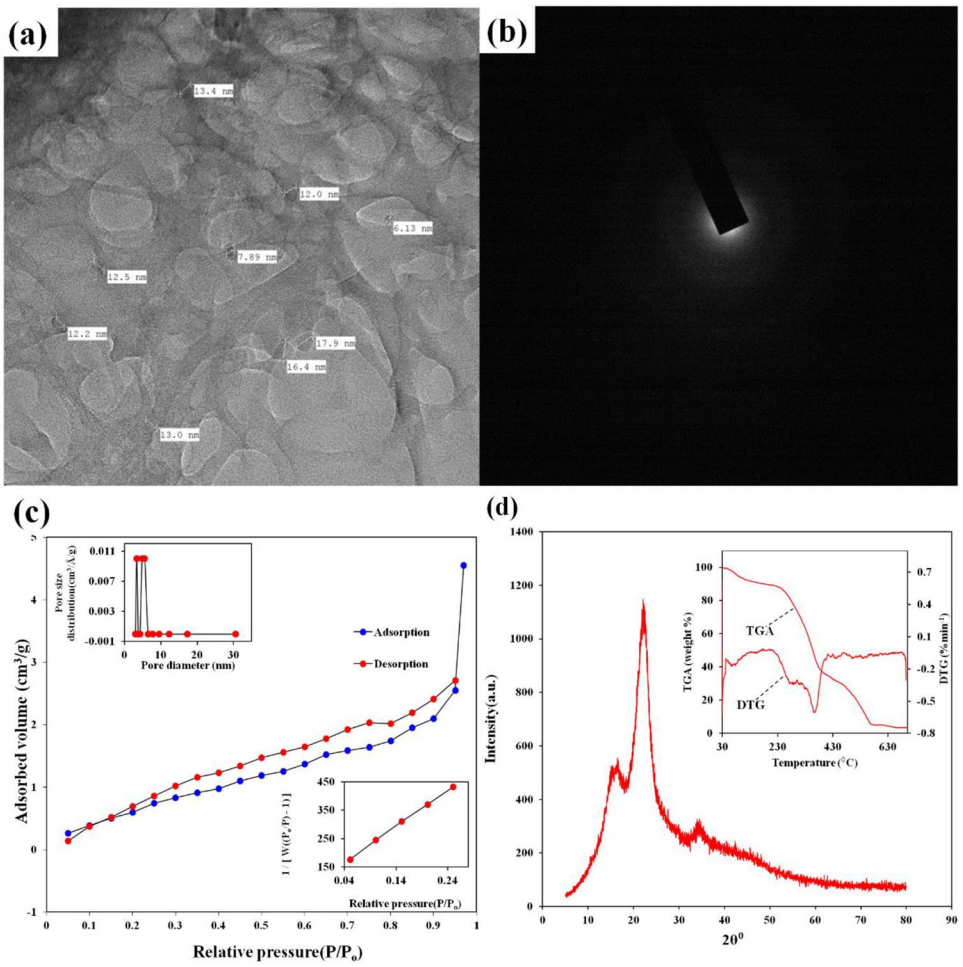

Fig. 2 **a** T.E.M. image of N.A.I.S.D. **b** S.A.E.D. pattern of N.A.I.S.D. **c** B.E.T. nitrogen adsorption–desorption isotherm at 77 K for N.A.I.S.D. (inset upper left, BJH pore size distribution adsorption plot of N.A.I.S.D.; inset lower right, multi-point B.E.T. plot of N.A.I.S.D.). **d** X.R.D. spectra of N.A.I.S.D. (inset, T.G.A.–D.T.G. curve of N.A.I.S.D.)

Table 2 Summary of B.E.T. surface area and pore analyses N.A.I.S.D.

Parameters	Values
BET surface area	3.149 $m^2\ g^{-1}$
Multipoint pore volume of the pore at $P/P_o = 0.15$	0.52 $cm^3\ g^{-1}$
BJH adsorption surface area	1.965 $m^2\ g^{-1}$
BJH adsorption pore volume	0.008 cc g^{-1}
BJH adsorption pore radius Dv(r)	17.062 Å
BJH desorption surface area	1.957 $m^2\ g^{-1}$
BJH desorption pore volume	0.008 cc g^{-1}
BJH desorption pore radius Dv(r)	17.053 Å

3.8.2 Effect of pH

The pH controls the degree of ionization, micropore surface charges, and dye fluid nature and is among the important guiding factor affecting adsorption performance of the adsorbent. The impact of pH on M.B. sequestration by A.I.S.D. and N.A.I.S.D. was investigated in the pH range of 2–13 at C_o of 100 mg L^{-1}. As shown in Fig. 3c, with a change in pH from 2 to 7, the q_e rose from 80.74 to 180.51 mg g^{-1} for A.I.S.D. and from 147.33 to 248.91 mg g^{-1} for N.A.I.S.D. Following that, a pH increase of 7 to 13 shows a slight improvement in adsorption capacity. The modified adsorbent (N.A.I.S.D.) has a greater adsorption capacity than the unmodified one (A.I.S.D.). This is owing to the fact that N.A.I.S.D. has larger vacant sites than A.I.S.D., resulting in enhanced M.B. adsorption for the N.A.I.S.D. At pH values higher than 7, cationic M.B. adsorption is preferred. It is because A.I.S.D./N.A.I.S.D. shows the presence of a negative charge on the surface and deprotonation of A.I.S.D./N.A.I.S.D.'s functional groups, resulting in the generation of hydrogen ions. As a result, the deprotonated groups serve as receptor sites for the cationic M.B., resulting in improved adsorption. The graph mirrored this, which shows that higher pH favors adsorption. The positively charged (or protonated) surface and the dye molecule show electrostatic repulsion, thus preventing effective adsorption at lower pH.

The point of zero charge (pH_{pzc}) of an adsorbent is a remarkable parameter to understand the substantial influence of pH on adsorption. With the help of the

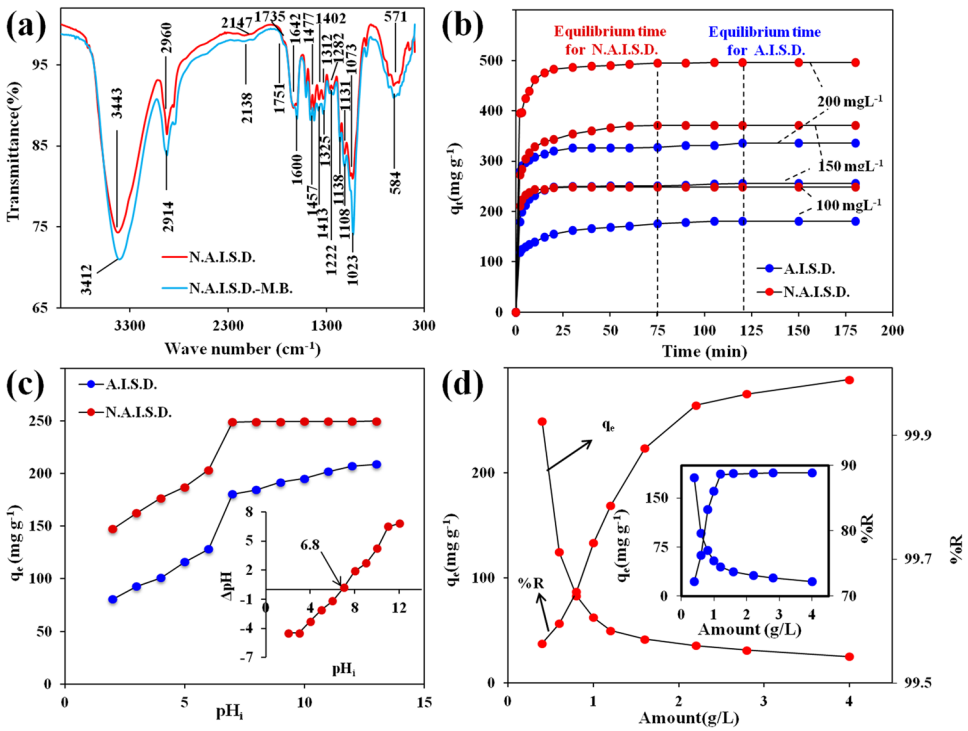

Fig. 3 **a** F.T.I.R. spectra of N.A.I.S.D. and N.A.I.S.D./M.B. **b** Effect of contact time on adsorption capacity at different initial dye concentration (C_o) and contact time. **c** Effect of pH on the adsorption capacity (inset—pH_{pzc} of N.A.I.S.D. adsorbent). **d** Effect of adsorbent dose on removal efficiency and adsorbent capacity of N.A.I.S.D. (inset—A.I.S.D.) at 303 K

solid-addition method, the pH_{pzc} of N.A.I.S.D. was established to be 6.8 (Fig. 3c-inset). At pH > pH_{pzc}, i.e., deprotonation results in a negative surface charge, but when pH < pH_{pzc}, due to protonation resulting in positive surface charge, and when pH = pH_{pzc}, the adsorbent surface has zero net charge. As a result, any basic dye preferentially adsorbed when the pH of the A.I.S.D. and N.A.I.S.D. was larger than pH_{pzc}. In light of these observations, a pH value of 7.0 was chosen with care.

3.8.3 Adsorbent dose

The adsorbent dosage is a significant parameter since it controls the adsorption performance in the effective elimination of contaminants. The doses ranging from 0.4 to 4.0 g L^{-1} for both adsorbents were used in the experiments. At equilibria, the % R of A.I.S.D. and N.A.I.S.D. improves from 72.20 to 88.84% and 99.56 to 99.99%, respectively, when the adsorbent dosage is increased from 0.4 to 4.0 g L^{-1} (Fig. 3d). The continuous enhancement % R with adsorbent dose is due to increase in surface area and the availability of more binding sites for adsorption. However, as indicated in Fig. 3d, an opposing trend in adsorption capacity was observed. At the lowest adsorbent dose (i.e., 0.4 g L^{-1}), the maximum adsorption capacity of 180.51 mg g^{-1} and 248.91 mg g^{-1} was observed for M.B. by both adsorbents, viz., A.I.S.D. and N.A.I.S.D., respectively. Therefore, in perspective, it is worth commenting that the higher adsorbent dose offers the interaction of adsorbent particles like amalgamation and aggregation, which cause the reduction in effective surface area per unit weight of the adsorbents. Figure 3d further shows that the adsorption capacity was significantly greater with N.A.I.S.D. in comparison with that of A.I.S.D.

3.9 Adsorption kinetics

The time-dependent experiments were conducted to evaluate the kinetics behind the adsorption of M.B. on the surface of A.I.S.D. and N.A.I.S.D. The pseudo-first-order (PsFO), pseudo-second-order (PsSO), Elovich (El), intraparticle diffusion (InPD), and liquid film diffusion (LiFD) models were employed to analyze the kinetic data. The linearized expressions of different kinetic models are given in Table 3 [42, 53].

Table 4 lists the kinetic parameters accompanying the adsorption of M.B. by A.I.S.D. and N.A.I.S.D. Based on R^2 values (close to unity) for t/q_t vs. t plot (Fig. 4a, b), it is clear that the PsSO model has an excellent fit for the adsorption of dye by both adsorbents. Furthermore, the calculated values of q_e (q_{cal}) using this approach are in excellent agreement with experimental ones (q_{exp}) for both raw and modified A.I.S.D. In reality, many researchers have already verified the PsSO kinetics for the elimination of M.B. by several adsorbents. The values of PsSO kinetics parameters associated with the adsorption of M.B. by a variety of adsorbents, as reported by other investigators, are summarized in Table 5.

The kinetics data were also assessed for the likelihood of M.B. adsorption via InPD onto the A.I.S.D. and N.A.I.S.D. The possibility of InPD being the sole rate-limiting step is indicated by the straight line plot of q_t vs. $t^{1/2}$ passing through the origin [54]. Because q_t vs. $t^{1/2}$ intercepts were non-zero (Table 4), it may be inferred that this model is unsuitable in the present case. Furthermore, ln (1 – F) vs. t had zero intercepts as D values ranging from – 1.947 to – 0.7793 for A.I.S.D. and – 4.2683 to – 2.3735 for N.A.I.S.D. (Table 4) point out the unsuitability of the LiFD model in the present case.

3.10 Adsorption isotherm

The process governing the confiscation of M.B. by A.I.S.D. and N.A.I.S.D. was analyzed by employing different isotherm models. This behavior of the adsorbate–adsorbent system has been defined using a variety of isotherm frameworks. The Langmuir (Lr), Freundlich (Fh), and Temkin (Tn) isotherm models were used to assess the obtained results for the isotherm investigation. The Lr model relies on the idea that every unoccupied space can be singly adsorbed, with little connection between adsorbed molecules. It focuses on single-layer adsorption. According to the Fh isotherm model, adsorption happens in a multilayered with a complex composition of adsorption sites. The Tn model specifies a declining adsorption heat as the surface of the adsorbent is covered by adsorbate molecules [75]. The linear isotherm equations for these models are listed in Table 6 [76].

Table 7 lists isotherm model parameter values obtained for the adsorption of M.B. by A.I.S.D. and N.A.I.S.D. Based on the values of the correlation coefficient (R^2), the Lr model was found to be suitable for the adsorption of M.B. by both adsorbents. The Fh and Tn isotherm frameworks have lower R^2 values indicating that they are not as applicable as Lr in the present case. The Lr model plots accompanying the adsorption by both the adsorbents are shown in Fig. 4c and d. The increase in values of q_m with the increase in temperature (Table 7) is owing to the endothermic nature of the process, as the adsorption was enhanced by the increase in temperature. A higher q_m value was obtained with N.A.I.S.D. than that for A.I.S.D. at each temperature.

Furthermore, a non-dimensional factor R_L ($= \frac{1}{1+K_L C_0}$), whose magnitude defines whether the operation is irreversible (0), linear (1), unfavorable (> 1), and favorable (0–1), was used to check the feasibility of the process. At 303 K, the values of R_L were 0.3537, 0.2673, 0.2148/0.0058, 0.0.0039, and 0.0029 for the adsorption of dye by A.I.S.D./N.A.I.S.D. at the initial dye concentration of 100, 150, and 200 mg L^{-1}, respectively. The fact that these numbers are in the 0–1 range confirms the favorable nature of adsorption.

According to an analysis of relevant literature, the Langmuir isotherm has already been found to be validated in the adsorption of M.B. by a range of adsorbents. Table 8 compares the Lr isotherm variables found in the current study with those previously documented for adsorption M.B. by other researchers.

3.11 Adsorption thermodynamics

The effect of temperature on the removal of M.B. by A.I.S.D. and N.A.I.S.D. was studied in the temperature range of 303–333 K. To examine the thermodynamics behind the adsorption, the values of changes in enthalpy (ΔH°), entropy (ΔS°), and Gibb's free energy (ΔG°) were determined by using following equations:

$$\Delta G^\circ = -RTInK_c \tag{12}$$

$$InK_c = \frac{-\Delta G^\circ}{RT} = \frac{-\Delta H^\circ}{RT} + \frac{\Delta S^\circ}{R} \tag{13}$$

where, K_c is the equilibrium constant. The values of ΔG° along with those of ΔS° and ΔH°, calculated from the slope and intercept of the ln K_c vs. 1/T plot (Fig. 4e, f), are listed in Table 9. The qualitative aspects of thermodynamics of M.B. adsorption via A.I.S.D. and N.A.I.S.D. were essentially the same in both cases. Table 9 clearly indicates that the feasibility of adsorption is much higher with N.A.I.S.D. than that with A.I.S.D. The better adsorption feasibility by N.A.I.S.D. over A.I.S.D. supports the better utility of the

Table 3 Kinetic equations and parameters (units) used

Kinetic models	Equations	Parameters (units)
PsFO	$\ln(q_e - q_t) = \ln q_e - K_1 t$	K_1 (min^{-1}): PsFO rate constant
PsSO	$\frac{t}{q_t} = \frac{1}{K_2 q_e^2} + \frac{t}{q_e}$	K_2 (g min^{-1} mg^{-1}): PsSO rate constant
El	$q_t = \frac{\ln(\alpha\beta)}{\beta} + \frac{1}{\beta}\ln t$	α (mg g^{-1} min^{-1}): initial adsorption rate β (g mg^{-1}): desorption constant
InPD	$q_t = K_{id} t^{1/2} + C$	K_{id} (mg $min^{-½}$ g^{-1}): InPD rate constant
LiFD	$\ln(1 - F) = -K_{fd} t + D$	K_{fd} (min^{-1}): LiFD rate constant $F = (q_t/q_e)$: achievement of fractional equilibrium D: LiFD constant

Table 4 Kinetic parameters for the confiscation of M.B. by A.I.S.D. and N.A.I.S.D. (experimental conditions: adsorbent dose = 0.4 g L^{-1}, T = 303 K, pH = 7, and t = 120 min for A.I.S.D. and 75 min for N.A.I.S.D.)

	A.I.S.D.				N.A.I.S.D.			
Initial dye concentration in mg L^{-1}								
	50	100	150	200	50	100	150	200
PsFO								
K_1	0.0172	0.0338	0.0270	0.0201	0.0109	0.0384	0.0481	0.045
q_{exp}	101.32	180.51	255.49	335.26	124.30	248.90	371.40	495.00
q_{cal}	15.65	39.02	21.35	23.44	4.154	1.02	47.47	39.09
R^2	0.9557	0.5596	0.5331	0.4232	0.2332	0.7887	0.4766	0.4584
PsSO								
K_2	0.004645	0.0021	0.004225	0.003333	0.0156	0.0177	0.0024	0.00307
q_{exp}	101.32	180.51	255.49	335.26	124.30	248.90	371.40	495.00
q_{cal}	101.01	181.82	256.41	335.26	125.00	250.00	370.37	500.00
R^2	0.9990	0.9995	1.0000	0.9999	0.9999	1.0000	0.9999	1.0000
InPD								
K_{id}	3.3722	8.0654	9.2903	10.500	6.3205	14.874	26.363	33.629
C	66.53	99.836	168.34	235.78	84.684	159	197.19	281.64
R^2	0.3612	0.5736	0.3822	0.3028	0.2550	0.3459	0.5170	0.4567
El								
β	0.10038	0.0430	0.0347	0.0307	0.0990	0.0433	0.02347	0.0187
α	27.4×10^{2}	6.17×10^{2}	30.78×10^{2}	14.36×10^{3}	38.83×10^{3}	20.08×10^{3}	37.82×10^{3}	90.26×10^{3}
R^2	0.4865	0.7348	0.5676	0.4475	0.3064	0.393	0.5946	0.5259
LiFD								
K_{fd}	0.0185	0.0465	0.0392	0.0282	0.0131	0.0229	0.0131	0.0163
D	−1.5804	−0.7793	−1.7061	−1.947	−2.3735	−4.2683	−2.3735	−2.8063
R^2	0.6513	0.8612	0.7768	0.7015	0.1759	0.1535	0.1735	0.2309

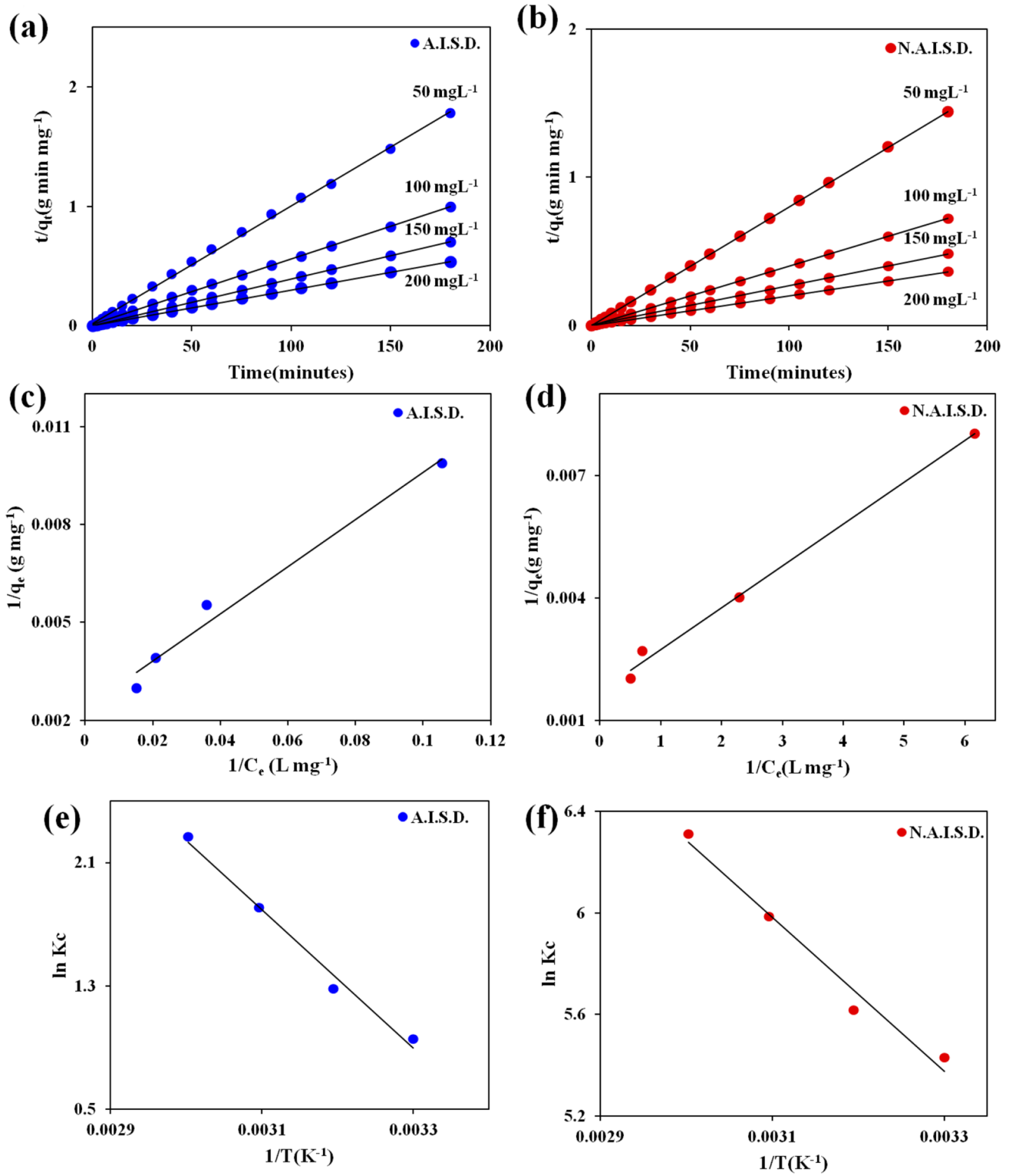

Fig. 4 PsSO kinetic plot for the adsorption of M.B. onto the **a** A.I.S.D. and **b** N.A.I.S.D. at different initial dye concentrations; Lr isotherm plot for the adsorption of M.B. onto **c** A.I.S.D. and **d** N.A.I.S.D. at 303 K; ln K_c vs. 1/T plot the adsorption of M.B. onto **e** A.I.S.D. and **f** N.A.I.S.D

Table 5 PsSO kinetic parameters for the adsorption of M.B. onto different adsorbents

Adsorbent	C_o (mg L^{-1})	M (g L^{-1})	K_2 (g $minmg^{-1}$)	q_e (mgg^{-1})	R^2	References
Magnetized *Tectona grandis* sawdust	50	1.0	0.00439	49.505	0.9904	[42]
Magnetized chitosan nanocomposite	50	1.2	0.0205	26.136	0.9694	[55]
Citrus limetta peel	50	2.0	0.0570	23.255	0.9999	[56]
K_2CO_3/olive pomace ash	100	0.3	1.4300	28.520	0.9600	[57]
Coconut husk activated carbon	100	0.03	0.144	83.33	1.0000	[58]
Alkali/*Metroxylon* spp.	300	0.1	0.000000428	146.07	0.9999	[59]
Alkali/Foumanat tea waste	100	0.5	0.220	34.25	1.0000	[60]
Citric acid/wheat straw	250	2.0	0.0117	9.268	0.9949	[61]
Citric acid/kenaf core fibers	100	1.0	0.00478	96.15	0.9990	[62]
NaOH/pine cone powder	20	0.015	0.0044	62.11	0.9991	[63]
Tartaric acid/bagasse/palm tree sawdust	250	0.4	1.50	54.99	0.8900	[64]
Tartaric acid/*Brassica napus* L	200	1.0	0.003797	172.4	0.9995	[65]
NaOH/*Leucaena leucocephala* leaf	30	1.0	0.001	71.43	0.9990	[66]
NaOH/rice husk	234	0.01	0.00102	459.00	0.97951	[67]
Eichhornia crassipes stem	300	0.01	0.0811	50.42	0.9999	[68]
Eichhornia crassipes leaf	300	0.01	0.0141	46.88	0.9999	[68]
Pine needle biochar	50	0.025	0.0032	37.31	0.9900	[69]
Strong acid/pine needle biochar	50	0.025	0.0167	76.92	1.0000	[69]
Weak acid/pine needle biochar	50	0.025	0.0022	49.02	0.9800	[69]
Bi/beech wood biochar	50	0.050	0.0120	92.953	0.9910	[70]
Bi/corncob biochar	50	0.05	0.006	42.381	0.9410	[70]
Bi/bamboo biochar	50	0.05	0.011	32.884	0.9580	[70]
KOH/sugarcane bagasse Activated carbon	50	0.08	0.00146	61.50	0.9900	[71]
Azolla-derived micro- and mesoporous carbon	400	0.005	0.000456	1647.98	0.9900	[72]
Eucalyptus bark/kaolin clay	20	0.04	0.097	22.62	0.9994	[73]
CoOx/*Enteromorpha* algae	100	0.002	0.00140	1176.5	0.9989	[74]
MoOy/*Enteromorpha* algae	100	0.002	0.00210	1190.5	0.9979	[74]
CoOx/MoOy/*Enteromorpha* algae	100	0.002	0.00160	1265.8	0.9971	[74]
A.I.S.D	100	0.4	0.00210	181.82	0.9995	Present work
N.A.I.S.D	100	0.4	0.01770	250.00	1.0000	Present work

Table 6 Adsorption isotherm equations and parameters (units) used

Isotherm framework	Equations	Parameters (units)
Lr	$\frac{1}{q_e}=\frac{1}{q_m K_L C_e}+\frac{1}{q_m}$	q_m (mg g^{-1}): maximum (complete) monolayer adsorption capacity K_L (L mg^{-1}): Langmuir adsorption constant
Fh	$\ln q_e=\frac{1}{n}\ln C_e+\ln K_F$	K_F ($mg^{1-1/n}$ $L^{1/n}$ g^{-1}): Freundlich constants incorporating the factors affecting the adsorption capacity and N: Freundlich constants incorporating the factors affecting adsorption intensity
Tn	$q_e=\frac{RT}{b}\ln C_e+\frac{RT}{b}\ln K_T$	K_T (L g^{-1}: Temkin isotherm constant B (=RT b^{-1}): constant related to the heat of adsorption b (J mol^{-1}): Temkin constant

former and points out its novelty. Furthermore, the thermodynamic feasibility increases with the increase of temperature with both adsorbents. This is due to an increase in the kinetic energy of the M.B. molecules with the rise in temperature. However, the process is less endothermic with N.A.I.S.D. The qualitative aspects regarding entropy change are the same with both adsorbents. The enhancement of entropy during adsorption is presumably due to the gain of translational entropy by the adsorbate molecules [77]. Literature indicates that a majority of researchers reported

Table 7 Isotherm parameters for the adsorption of M.B. onto A.I.S.D. and N.A.I.S.D. at different temperatures (experimental conditions: $pH = 7$, adsorbent dose = 0.4 g L^{-1}, $t = 120$ min for A.I.S.D. and 75 min for N.A.I.S.D.)

	A.I.S.D.				N.A.I.S.D.			
T (°C)	30	40	50	60	30	40	50	60
Lr								
q_m	416.67	434.78	454.54	476.19	588.23	625.00	666.66	714.28
K_L	0.03315	0.00609	0.00637	0.0500	1.7006	0.2750	0.07142	2.0040
R^2	0.9973	0.9829	0.9834	0.9871	0.9947	0.9906	0.9913	0.9929
Fh								
N	1.124	1.163	1.1603	1.178	1.95	1.153	1.141	1.124
K_F	8.354	3.529	3.803	26.039	336.90	134.464	335.52	865.40
R^2	0.9815	0.9706	0.9716	0.9800	0.974	0.9863	0.9874	0.9891
Tn								
B	162.25	37.341	38.047	44.245	135.45	46.354	46.804	82.516
K_T	0.1109	0.2008	0.2158	1.6788	14.669	10.709	29.725	82.516
R^2	0.9878	0.947	0.9482	0.9677	0.958	0.9841	0.9800	0.9723

entropy escalation during the adsorption of M.B. by different adsorbents. The qualitative changes in thermodynamic parameters accompany the adsorption of M.B. by different adsorbents, as reported by other investigators, are compiled in Table S1. Our results are in qualitative agreement with those reported with the majority of other adsorbents.

3.12 Adsorption mechanism

The scheme behind the adsorption pathway must be comprehended to look within it. However, before understanding the mechanism of M.B. dye adsorption, two key factors must be considered: first, the geometry and type of the adsorbate, and second, the adsorbent surface qualities. The major components of A.I.S.D. and N.A.I.S.D., as shown in Table 1, are cellulose, hemicellulose, and lignin, as well as some minor constituents.

Both cellulose and hemicellulose contain oxygen functional groups such as hydroxyl, ether, and carbonyl, while lignin is a complex and highly aromatic substance and acts as a cementing agent that holds both cellulose and hemicelluloses units [53]. The lignin fraction of A.I.S.D. is reduced by chemical treatment with NaOH, which increases the cellulose content in N.A.I.S.D. (Table 1). As a result, the number of binding sites increased. Additionally, S.E.M./E.D.X.S. and B.E.T. tests simply illustrate that modification eliminates the contaminants, improves morphology, and increases surface area. Thus, dye molecules were easily permeated into the pores of N.A.I.S.D.

In A.I.S.D. and N.A.I.S.D., the presence and participation of -OH, -C = O, and $–NR_2$ groups in binding M.B. molecules have been highlighted based on F.T.I.R. investigations. The increased adsorption of N.A.I.S.D. over A.I.S.D. may be due to the formation of hydrogen bonds between -OH groups present on the adsorbent surface and the nitrogen atoms of the dye molecule. A similar mechanism was proposed for the adsorption of crystal violet on a NaOH-treated rice husk surface [78]. Furthermore, the electrostatic force that exists between negatively charged surface functional groups and the positive charge core of M.B. molecules may play active role in adsorption. Furthermore, at $pH > pH_{pzc}$, the surface becomes strongly negatively charged due to the deprotonation of functional groups and therefore acts as a strong bonding site for cationic dye. These different possible interactions are shown in Fig. 5.

3.13 Desorption

Desorption studies were performed on five desorbing agents (0.1 M of NaOH, HCl, CH_3COOH, NaCl, and DM-DW). The best desorption of M.B. from A.I.S.D. and N.A.I.S.D. was observed with 0.1 M HCl. With 0.1 M HCl, the optimum

Table 8 Lr isotherm parameters for the adsorption of M.B. onto different adsorbents

Composite adsorbents	M (g L^{-1})	K_L (Lmg^{-1})	q_m (mg g^{-1})	R^2	References
Magnetized *Tectona grandis* sawdust	1.0	0.15760	172.410	0.9987	[42]
Magnetized chitosan nanocomposite	1.2	0.30751	76.335	0.9921	[55]
Citrus limetta peel	2.0	0.02880	227.300	0.9787	[56]
K_2CO_3/olive pomace boiler ash	0.3	0.29000	149.110	0.9700	[57]
Coconut husk activated carbon	0.03	0.28600	500.00	0.9990	[58]
Alkali/*Metroxylon* spp.	0.1	0.55000	212.80	0.9979	[59]
Acid/*Metroxylon* spp.	0.1	0.10100	36.82	0.9488	[59]
Alkali/Foumanat tea waste	0.5	0.0082	404.72	0.9999	[60]
Citric acid/wheat straw	2.0	0.2689	312.50	0.9975	[61]
Citric acid/kenaf core fibers	1.0	0.011	103.1	0.994	[62]
Base/pine cone powder	0.015	0.2734	142.86	0.9955	[63]
Tartaric acid/bagasse	0.4	0.85	59.88	0.9900	[64]
Tartaric acid/*Brassica napus* L	1.0	0.11600	246.4	0.9916	[65]
NaOH treated *Leucaena leucocephala* leaf powder	1.0	1.0000	208.33	0.9850	[66]
NaOH/rice husk	0.01	0.67540	552.50	0.9931	[67]
Eichhornia crassipes stem	0.01	0.02400	153.84	0.9935	[68]
Eichhornia crassipes leaf	0.01	0.01700	153.84	0.9848	[68]
Pine needle biochar	0.025	0.23000	106.38	0.9800	[69]
Strong acid/pine needle biochar	0.025	0.29000	153.84	0.9900	[69]
Weak acid/pine needle biochar	0.025	0.14000	113.63	0.9800	[69]
Bi/beech wood biochar	0.05	0.13500	178.590	0.9950	[70]
Bi/corncob biochar	0.05	0.04800	81.820	0.9510	[70]
Bi/bamboo biochar	0.05	0.02900	59.820	0.9900	[70]
Azolla-derived micro- and mesoporous carbon	0.005	77.9000	1930.0	0.9700	[72]
Eucalyptus bark/kaolin clay	0.04	0.40000	74.630	0.9946	[73]
CoOx/*Enteromorpha* algae	0.002	0.00307	1351.40	0.9974	[74]
MoOy/*Enteromorpha* algae	0.002	0.00377	1298.70	0.9998	[74]
CoOx/MoOy/*Enteromorpha* algae	0.002	0.00176	1587.30	0.9987	[74]
A.I.S.D	0.4	0.03315	416.67	0.9793	Present work
N.A.I.S.D.	0.4	1.7006	588.23	0.9947	Present work

Table 9 Thermodynamics parameters (experimental conditions: $pH = 7$, $t = 120$ min for A.I.S.D. and 75 min for N.A.I.S.D., adsorbent dose = 0.04 g L^{-1}, and $C_o = 100$ mg L^{-1})

A.I.S.D.					N.A.I.S.D.			
T (°C)	30	40	50	60	30	40	50	60
-ΔG° (kJ mol^{-1})	2.4048	3.3367	4.860	6.2784	13.680	14.619	16.076	17.477
ΔH° (kJ mol^{-1})			37.381		25.208			
ΔS° (J K^{-1} mol^{-1})			130.82		127.90			

desorption of M.B. from both A.I.S.D. and N.A.I.S.D. was observed. Since the removal process might be more economical and practical if the adsorbents have the potential to be successfully reused in several consecutive cycles, the present investigation explored this possibility. Given this fact, four adsorption–desorption cycles have been carried out with 0.1 M HCl; the findings are illustrated in Fig. 6. This figure confirms that adsorbents can be effectively used in at least four repeated cycles for the removal of M.B. dye from aqueous solution. The comparatively reduced desorption from N.A.I.S.D. over A.I.S.D. is owing to the strong binding potential of the former with M.B. Similar results were reported with NaOH-modified fishbone charcoal adsorbent used to remove M.B. dye [79]. The potential of the present adsorbents for their repeated application in the dye removal process reduces the problems of disposal of used adsorbents and dye-contaminated water, thereby making the process economical.

4 Conclusion

The current study looks at the improved performance of A.I.S.D. after it was modified with NaOH to remove M.B. dye from an aqueous phase. The adsorption capacity for both the adsorbents (A.I.S.D. and N.A.I.S.D.) has been influenced by batch parameters, and the equilibrium for optimum adsorption was attained in 120 min for A.I.S.D. and 75 min for N.A.I.S.D. The Langmuir isotherm was best fitted to the adsorption data with the maximum monolayer adsorption capacity of 416.67 mg g^{-1} and 588.23 mg g^{-1} for A.I.S.D. and N.A.I.S.D., respectively. The kinetics data presented the applicability of the PsSO model accompanying the adsorptive removal of M.B. by both adsorbents, A.I.S.D. and N.A.I.S.D. The thermodynamic studies suggested that the adsorption of M.B. by both adsorbents was spontaneous, endothermic, and accompanied by an increase in entropy. The best desorption of M.B. from M.B.-loaded A.I.S.D. and N.A.I.S.D. was with 0.1 M HCl. The present adsorbents were found to be recyclable for at least four cycles. In view of the efficient and economical removal of M.B. from contaminated water and the reusability of adsorbent in several cycles, the current study claims that N.A.I.S.D. adsorbent is novel, cheap, and economically appropriate for the remediation of dye-polluted water. The AISD-based adsorbents have the potential for further modification with other suitable agents. There is scope for developing AISD-based adsorbents to extend their applicability in wastewater remediation containing a variety of contaminants, like anionic dyes, heavy metal ions, drugs, pesticides, etc. Furthermore, the separation of adsorbent is a serious and challenging issue during the adsorptive treatment of wastewater. Since magnetic separation is fast, time-saving, and cost-effective, magnetic modification and chemical modification might be potential scope for further investigations.

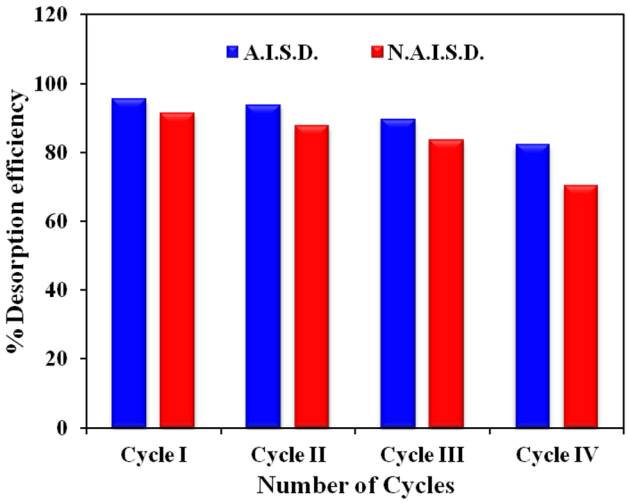

Fig. 6 Desorption of M.B. from M.B. loaded A.I.S.D. and N.A.I.S.D

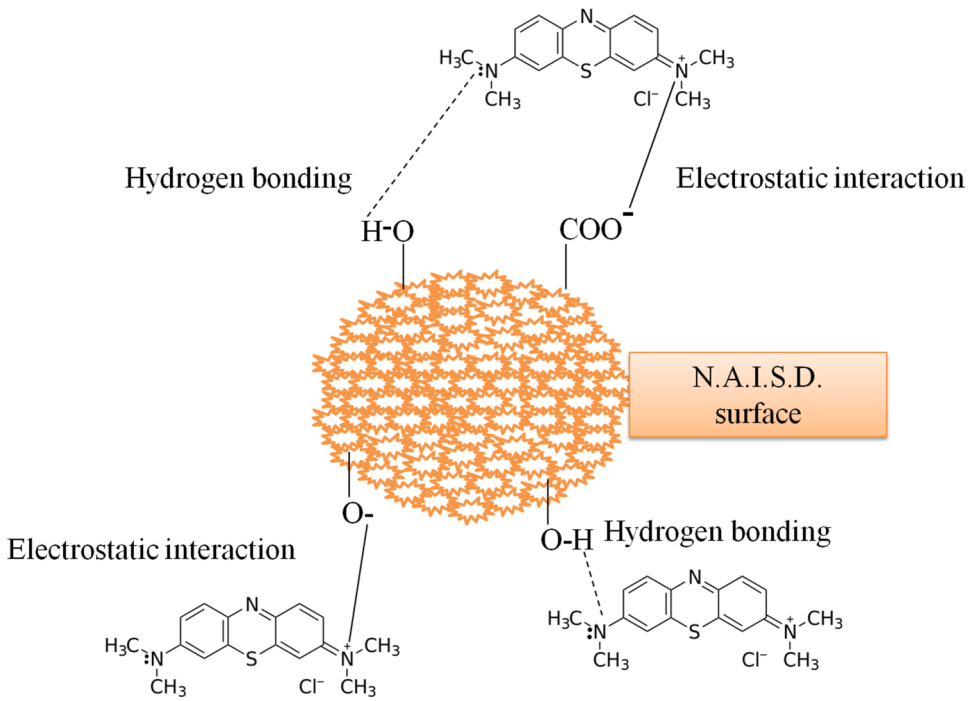

Fig. 5 Plausible interactions accompanying the adsorption of M.B. onto N.A.I.S.D.

Supplementary Information The online version contains supplementary material available at https://doi.org/10.1007/s13399-023-04161-5.

Acknowledgements The authors thank the Department of Applied Chemistry, Faculty of Engineering and Technology, Aligarh Muslim University, for extending laboratory facilities.

Author contribution ZH performed the experiments. AN supervised the work. MA, FM, and AN analyzed and interpreted the experimental data. ZA wrote the first draft. MA, FM, and AN assisted ZA in writing the final manuscript. All the authors discussed the data/draft and agreed to submit the manuscript.

Data availability Not applicable.

Declarations

Ethical approval Not applicable.

Competing interests The authors declare no competing interests.

References

1. Chuah LF, Chew KW, Bokhari A et al (2022) Biodegradation of crude oil in seawater by using a consortium of symbiotic bacteria. Environ Res 213:113721. https://doi.org/10.1016/j.envres.2022.113721
2. Chuah LF, Mokhtar K, MhdRuslan SM et al (2023) Implementation of the energy efficiency existing ship index and carbon intensity indicator on domestic ship for marine environmental protection. Environ Res 222:115348. https://doi.org/10.1016/j.envres.2023.115348
3. Cherniwchan J (2012) Economic growth, industrialization, and the environment. Resour Energy Econ 34:442–467. https://doi.org/10.1016/j.reseneeco.2012.04.004
4. Bharagava RN, Saxena G, Mulla SI (2020) Introduction to industrial wastes containing organic and inorganic pollutants and bioremediation approaches for environmental management. Bioremediation Ind Waste Environ Saf 1–18. https://doi.org/10.1007/978-981-13-1891-7_1
5. Elgarahy AM, Elwakeel KZ, Mohammad SH, Elshoubaky GA (2021) A critical review of biosorption of dyes, heavy metals and metalloids from wastewater as an efficient and green process. Clean Eng Technol 4:100209. https://doi.org/10.1016/j.clet.2021.100209
6. Jadhav JP, Kalyani DC, Telke AA et al (2010) Evaluation of the efficacy of a bacterial consortium for the removal of color, reduction of heavy metals, and toxicity from textile dye effluent. Bioresour Technol 101:165–173. https://doi.org/10.1016/j.biortech.2009.08.027
7. Schwarzenbach RP, Egli T, Hofstetter TB et al (2010) Global water pollution and human health. Annu Rev Environ Resour 35:109–136. https://doi.org/10.1146/annurev-environ-100809-125342
8. Gürses A, Açıkyıldız M, Güneş K, Gürses MS (2016) Classification of dye and pigments. In: Dyes and pigments. SpringerBriefs in Molecular Science. Springer, Cham. pp 31–45
9. Wainwright M (2008) Dyes in the development of drugs and pharmaceuticals. Dye Pigment 76:582–589. https://doi.org/10.1016/j.dyepig.2007.01.015
10. Verma AK, Dash RR, Bhunia P (2012) A review on chemical coagulation/flocculation technologies for removal of colour from textile wastewaters. J Environ Manage 93:154–168. https://doi.org/10.1016/j.jenvman.2011.09.012
11. Kant R (2012) Textile dyeing industry an environmental hazard. Nat Sci 04:22–26. https://doi.org/10.4236/ns.2012.41004
12. Dailin DJ, Nordin NZ, Tan LT et al (2022) State of the art bioremediation of textile dye in wastewater: a review. Biosci Res 19:914–924
13. Deshannavar UBB, Ratnamala GMM, Kalburgi PBB et al (2016) Optimization, kinetic and equilibrium studies of disperse yellow 22 dye removal from aqueous solutions using Malaysian teak wood sawdust as adsorbent. Indian Chem Eng 58:12–28. https://doi.org/10.1080/00194506.2014.987831
14. Mashkoor F, Nasar A (2021) Environmental application of agro-waste derived materials for the treatment of dye-polluted water: a review. Curr Anal Chem 17:904–916. https://doi.org/10.2174/1573411016666200102114854
15. Dutta S, Gupta B, Srivastava SK, Gupta AK (2021) Recent advances on the removal of dyes from wastewater using various adsorbents: a critical review. Mater Adv 2:4497–4531. https://doi.org/10.1039/D1MA00354B
16. Pang YL, Abdullah AZ (2013) Current status of textile industry wastewater management and research progress in Malaysia: a review. CLEAN - Soil, Air, Water 41:751–764. https://doi.org/10.1002/clen.201000318
17. Kausar A, Zohra ST, Ijaz S et al (2022) Cellulose-based materials and their adsorptive removal efficiency for dyes: a review. Int J Biol Macromol. https://doi.org/10.1016/j.ijbiomac.2022.10.220
18. Yagub MT, Sen TK, Afroze S, Ang HM (2014) Dye and its removal from aqueous solution by adsorption: a review. Adv Colloid Interface Sci 209:172–184. https://doi.org/10.1016/j.cis.2014.04.002
19. Crini G, Lichtfouse E (2019) Advantages and disadvantages of techniques used for wastewater treatment. Environ Chem Lett 17:145–155
20. Kushwaha S, Soni H, Ageetha V, Padmaja P (2013) An insight into the production, characterization, and mechanisms of action of low-cost adsorbents for removal of organics from aqueous solution. Crit Rev Environ Sci Technol 43:443–549. https://doi.org/10.1080/10643389.2011.604263
21. Bulgariu L, Escudero LB, Bello OS et al (2019) The utilization of leaf-based adsorbents for dyes removal: a review. J Mol Liq 276:728–747. https://doi.org/10.1016/j.molliq.2018.12.001
22. Crini G (2006) Non-conventional low-cost adsorbents for dye removal: a review. Bioresour Technol 97:1061–1085. https://doi.org/10.1016/j.biortech.2005.05.001
23. Rafatullah M, Sulaiman O, Hashim R, Ahmad A (2010) Adsorption of methylene blue on low-cost adsorbents: a review. J Hazard Mater 177:70–80. https://doi.org/10.1016/j.jhazmat.2009.12.047
24. Shelke BN, Jopale MK, Kategaonkar AH (2022) Exploration of biomass waste as low cost adsorbents for removal of methylene blue dye: a review. J Indian Chem Soc 99:100530. https://doi.org/10.1016/j.jics.2022.100530
25. Gupta VK, Suhas (2009) Application of low-cost adsorbents for dye removal – a review. J Environ Manage 90:2313–2342. https://doi.org/10.1016/j.jenvman.2008.11.017
26. Zhou C, Wang Y (2020) Recent progress in the conversion of biomass wastes into functional materials for value-added applications. Sci Technol Adv Mater 21:787–804. https://doi.org/10.1080/14686996.2020.1848213
27. Malik DS, Jain CK, Yadav AK (2017) Removal of heavy metals from emerging cellulosic low-cost adsorbents: a review. Appl Water Sci 7:2113–2136. https://doi.org/10.1007/s13201-016-0401-8
28. Hussain MS, Rehman R, Imran M et al (2022) Eco-friendly detoxification of congo red dye from water by citric acid activated

bioadsorbents consisting of watermelon and water chestnuts peels collected from indigenous resources. Adsorpt Sci Technol 2022:1–20. https://doi.org/10.1155/2022/9056288
29. Singh AK, Ketan K, Singh JK (2017) Simple and green fabrication of recyclable magnetic highly hydrophobic sorbents derived from waste orange peels for removal of oil and organic solvents from water surface. J Environ Chem Eng 5:5250–5259. https://doi.org/10.1016/j.jece.2017.09.060
30. Machado Garcia R, Carleer R, Arada Pérez M et al (2022) Adsorption of Cibacron Yellow F-4G dye onto activated carbons obtained from peanut hull and rice husk: kinetics and equilibrium studies. Biomass Convers Biorefinery 12:323–339. https://doi.org/10.1007/s13399-020-00699-w
31. Mittal A, Teotia M, Soni RK, Mittal J (2016) Applications of egg shell and egg shell membrane as adsorbents: a review. J Mol Liq 223:376–387. https://doi.org/10.1016/j.molliq.2016.08.065
32. Nasar A (2023) Utilization of tea wastes for the removal of toxic dyes from polluted water—a review. Biomass Convers Biorefinery 13:1399–1415. https://doi.org/10.1007/s13399-020-01205-y
33. Basu M, Guha AK, Ray L (2017) Adsorption of lead on cucumber peel. J Clean Prod 151:603–615. https://doi.org/10.1016/j.jclepro.2017.03.028
34. Zainuddin MF, Shamsudin R, Mokhtar MN, Ismail D (2014) Physicochemical properties of pineapple plant waste fibers from the leaves and stems of different varieties. BioResources 9:. https://doi.org/10.15376/biores.9.3.5311-5324
35. Joshua JA, Ahiekpor JC, Kuyea A (2016) Nigerian hardwood (Nesogordonia papaverifera) sawdust characterization: proximate analysis, cellulose and lignin contents. Lignocellulose 5:50–58
36. Basu M, Guha AK, Ray L (2017) Adsorption behavior of cadmium on husk of lentil. Process Saf Environ Prot 106:11–22. https://doi.org/10.1016/j.psep.2016.11.025
37. Saldarriaga JF, Montoya NA, Estiati I, et al (2021) Unburned material from biomass combustion as low-cost adsorbent for amoxicillin removal from wastewater. J Clean Prod 284:. https://doi.org/10.1016/j.jclepro.2020.124732
38. Ahamad Z, Nasar A (2023) Utilization of Azadirachta indica sawdust as a potential adsorbent for the removal of crystal violet dye. Sustain Chem 4:110–126. https://doi.org/10.3390/suschem4010009
39. Shaaban A, Se S-M, Mitan NMM, Dimin MF (2013) Characterization of biochar derived from rubber wood sawdust through slow pyrolysis on surface porosities and functional groups. Procedia Eng 68:365–371. https://doi.org/10.1016/j.proeng.2013.12.193
40. Wang Z, Cao J, Wang J (2009) Pyrolytic characteristics of pine wood in a slowly heating and gas sweeping fixed-bed reactor. J Anal Appl Pyrolysis 84:179–184. https://doi.org/10.1016/j.jaap.2009.02.001
41. Sidiras D, Batzias F, Schroeder E et al (2011) Dye adsorption on autohydrolyzed pine sawdust in batch and fixed-bed systems. Chem Eng J 171:883–896. https://doi.org/10.1016/j.cej.2011.04.029
42. Mashkoor F, Nasar A (2020) Magnetized Tectona grandis sawdust as a novel adsorbent: preparation, characterization, and utilization for the removal of methylene blue from aqueous solution. Cellulose 27:2613–2635. https://doi.org/10.1007/s10570-019-02918-8
43. Jiang ZH, Yang Z, So CL, Hse CY (2007) Rapid prediction of wood crystallinity in Pinus elliotii plantation wood by near-infrared spectroscopy. J Wood Sci 53:449–453. https://doi.org/10.1007/s10086-007-0883-y
44. Zhang M, Zhang S, Chen Z et al (2019) Preparation and characterization of superabsorbent polymers based on sawdust. Polymers (Basel) 11:1891. https://doi.org/10.3390/polym11111891
45. CastroNapoli, N et al (2019) Massaranduba sawdust: a potential source of charcoal and activated carbon. Polymers (Basel) 11:1276. https://doi.org/10.3390/polym11081276
46. Mamaeva A, Tahmasebi A, Tian L, Yu J (2016) Microwave-assisted catalytic pyrolysis of lignocellulosic biomass for production of phenolic-rich bio-oil. Bioresour Technol 211:382–389. https://doi.org/10.1016/j.biortech.2016.03.120
47. Wu Z, Wang S, Zhao J et al (2014) Synergistic effect on thermal behavior during co-pyrolysis of lignocellulosic biomass model components blend with bituminous coal. Bioresour Technol 169:220–228. https://doi.org/10.1016/j.biortech.2014.06.105
48. Zabeti M, Baltrusaitis J, Seshan K (2016) Chemical routes to hydrocarbons from pyrolysis of lignocellulose using Cs promoted amorphous silica alumina catalyst. Catal Today 269:156–165. https://doi.org/10.1016/j.cattod.2015.11.024
49. Yang H, Yan R, Chen H et al (2007) Characteristics of hemicellulose, cellulose and lignin pyrolysis. Fuel 86:1781–1788. https://doi.org/10.1016/j.fuel.2006.12.013
50. Mishra RK, Mohanty K (2018) Pyrolysis kinetics and thermal behavior of waste sawdust biomass using thermogravimetric analysis. Bioresour Technol 251:63–74. https://doi.org/10.1016/j.biortech.2017.12.029
51. Chen Z, Hu M, Zhu X et al (2015) Characteristics and kinetic study on pyrolysis of five lignocellulosic biomass via thermogravimetric analysis. Bioresour Technol 192:441–450. https://doi.org/10.1016/j.biortech.2015.05.062
52. Ahmad A, Rafatullah M, Sulaiman O et al (2009) Scavenging behaviour of meranti sawdust in the removal of methylene blue from aqueous solution. J Hazard Mater 170:357–365. https://doi.org/10.1016/j.jhazmat.2009.04.087
53. Chowdhury S, Mishra R, Saha P, Kushwaha P (2011) Adsorption thermodynamics, kinetics and isosteric heat of adsorption of malachite green onto chemically modified rice husk. Desalination 265:159–168. https://doi.org/10.1016/j.desal.2010.07.047
54. Doğan M, Abak H, Alkan M (2009) Adsorption of methylene blue onto hazelnut shell: kinetics, mechanism and activation parameters. J Hazard Mater 164:172–181. https://doi.org/10.1016/j.jhazmat.2008.07.155
55. Mashkoor F, Nasar A, Jeong C (2022) Magnetized chitosan nanocomposite as an effective adsorbent for the removal of methylene blue and malachite green dyes. Biomass Convers Biorefinery. https://doi.org/10.1007/s13399-021-02282-3
56. Shakoor S, Nasar A (2016) Removal of methylene blue dye from artificially contaminated water using citrus limetta peel waste as a very low cost adsorbent. J Taiwan Inst Chem Eng 66:154–163. https://doi.org/10.1016/j.jtice.2016.06.009
57. Marrakchi F, Bouaziz M, Hameed BH (2017) Adsorption of acid blue 29 and methylene blue on mesoporous K_2CO_3-activated olive pomace boiler ash. Colloids Surfaces A Physicochem Eng Asp 535:157–165. https://doi.org/10.1016/j.colsurfa.2017.09.014
58. AL-Aoh HA, Yahya R, Jamil Maah M, Radzi Bin Abas M (2014) Adsorption of methylene blue on activated carbon fiber prepared from coconut husk: isotherm, kinetics and thermodynamics studies. Desalin Water Treat 52:6720–6732. https://doi.org/10.1080/19443994.2013.831794
59. Amode JO, Santos JH, Md. Alam Z, et al (2016) Adsorption of methylene blue from aqueous solution using untreated and treated (Metroxylon spp.) waste adsorbent: equilibrium and kinetics studies. Int J Ind Chem 7:333–345. https://doi.org/10.1007/s40090-016-0085-9
60. EbrahimianPirbazari A, Saberikhah E, Badrouh M, Emami MS (2014) Alkali treated Foumanat tea waste as an efficient adsorbent for methylene blue adsorption from aqueous solution. Water Resour Ind 6:64–80. https://doi.org/10.1016/j.wri.2014.07.003
61. Gong R, Zhu S, Zhang D et al (2008) Adsorption behavior of cationic dyes on citric acid esterifying wheat straw: kinetic and thermodynamic profile. Desalination 230:220–228. https://doi.org/10.1016/j.desal.2007.12.002
62. Sajab MS, Chia CH, Zakaria S et al (2011) Citric acid modified kenaf core fibres for removal of methylene blue from aqueous solution. Bioresour Technol 102:7237–7243. https://doi.org/10.1016/j.biortech.2011.05.011

63. Yagub MT, Sen TK, Ang M (2014) Removal of cationic dye methylene blue (MB) from aqueous solution by ground raw and base modified pine cone powder. Environ Earth Sci 71:1507–1519. https://doi.org/10.1007/s12665-013-2555-0
64. Low LW, Teng TT, Rafatullah M et al (2013) Adsorption studies of methylene blue and malachite green from aqueous solutions by pretreated lignocellulosic materials. Sep Sci Technol 48:1688–1698. https://doi.org/10.1080/01496395.2012.756912
65. Feng Y, Zhou H, Liu G et al (2012) Methylene blue adsorption onto swede rape straw (Brassica napus L.) modified by tartaric acid: equilibrium, kinetic and adsorption mechanisms. Bioresour Technol 125:138–144. https://doi.org/10.1016/j.biortech.2012.08.128
66. MegatHanafiah MAK, Mansur NF, Wan Ab Rahman WMN, Ismail M (2015) Methylene blue adsorption onto NaOH treated Leucaena leucocephala leaf power. Appl Mech Mater 752–753:251–256. https://doi.org/10.4028/www.scientific.net/AMM.752-753.251
67. Chen Y, Zhai SR, Liu N et al (2013) Dye removal of activated carbons prepared from NaOH-pretreated rice husks by low-temperature solution-processed carbonization and H3PO4 activation. Bioresour Technol 144:401–409. https://doi.org/10.1016/j.biortech.2013.07.002
68. Carneiro MT, Barros AZB, Morais AIS et al (2022) Application of water hyacinth biomass (Eichhornia crassipes) as an adsorbent for methylene blue dye from aqueous medium: kinetic and isothermal study. Polymers (Basel) 14:2732. https://doi.org/10.3390/polym14132732
69. Pandey D, Daverey A, Dutta K et al (2022) Valorization of waste pine needle biomass into biosorbents for the removal of methylene blue dye from water: kinetics, equilibrium and thermodynamics study. Environ Technol Innov 25:102200. https://doi.org/10.1016/j.eti.2021.102200
70. Li P, Su Y, Hu Z et al (2022) Adsorption of methylene blue by bismuth impregnated biochar of different biomass materials: pore structure and surface chemistry characteristics. J Chem Technol Biotechnol 97:2871–2880. https://doi.org/10.1002/jctb.7159
71. Jawad AH, Abdulhameed AS, Bahrudin NN et al (2021) Microporous activated carbon developed from KOH activated biomass waste: surface mechanistic study of methylene blue dye adsorption. Water Sci Technol 84:1858–1872. https://doi.org/10.2166/wst.2021.355
72. MotejaddedEmrooz HB, Maleki M, Rashidi A, Shokouhimehr M (2020) Adsorption mechanism of a cationic dye on a biomass-derived micro- and mesoporous carbon: structural, kinetic, and equilibrium insight. Biomass Convers Biorefinery 11:943–954. https://doi.org/10.1007/s13399-019-00584-1
73. Tan TCN, Sen TK (2020) Aqueous-phase methylene blue (MB) dye removal by mixture of eucalyptus bark (EB) biomass and kaolin clay (KC) adsorbents: kinetics, thermodynamics, and isotherm modeling. Sep Sci Technol 55:1036–1050. https://doi.org/10.1080/01496395.2019.1580734
74. Yang L, Wang Y, Liu A, Zhang Y (2019) CoOx/MoOy-anchored multi-wrinkled biomass carbon as a promising material for rapidly selective methyl blue removal. J Mater Sci 54:11024–11036. https://doi.org/10.1007/s10853-019-03612-7
75. Acemioğlu B (2022) Removal of a reactive dye using NaOH-activated biochar prepared from peanut shell by pyrolysis process. Int J Coal Prep Util 42:671–693. https://doi.org/10.1080/19392699.2019.1644326
76. Kayranli B (2011) Adsorption of textile dyes onto iron based waterworks sludge from aqueous solution; isotherm, kinetic and thermodynamic study. Chem Eng J 173:782–791. https://doi.org/10.1016/j.cej.2011.08.051
77. Kyzas GZ, Lazaridis NK, Mitropoulos AC (2012) Removal of dyes from aqueous solutions with untreated coffee residues as potential low-cost adsorbents: equilibrium, reuse and thermodynamic approach. Chem Eng J 189–190:148–159. https://doi.org/10.1016/j.cej.2012.02.045
78. Chakraborty S, Chowdhury S, Das Saha P (2011) Adsorption of crystal violet from aqueous solution onto NaOH-modified rice husk. Carbohydr Polym 86:1533–1541. https://doi.org/10.1016/j.carbpol.2011.06.058
79. Wang W, Liu Y, Chen X, Song S (2018) Facile synthesis of NaOH-modified fishbone charcoal (FBC) with remarkable adsorption towards methylene blue. Procedia Eng 211:495–505. https://doi.org/10.1016/j.proeng.2017.12.041